J Solid State Electrochem (2005) 9: 512–519
DOI 10.1007/s10008-004-0614-x

ORIGINAL PAPER

Dusan Losic · Joe G. Shapter · J. Justin. Gooding

Mapping of defects in self-assembled monolayers by polymer decoration

Received: 8 June 2004 / Revised: 15 October 2004 / Accepted: 18 October 2004 / Published online: 10 December 2004
© Springer-Verlag 2004

Abstract A new method mapping the defects in self-assembled monolayers (SAMs) is described. The method is based on electrochemical polymerisation of nonconductive tyramine in defect sites of a monolayer and subsequent visualisation of the polymer structures by atomic force microscopy (AFM). SAMs of hexadecanthiol (HDT) on gold prepared by deposition from solution and microcontact printing were used as a model for this study. The method allows easy mapping of defects on monolayers and provides information about their shape, size, size distribution, defect density and spatial distribution. Comparative electrochemical characterisation of defects in SAMs before and after polymerisation shows that polymer growth occurs on the sites of uncovered gold. The approach should be applicable for the characterisation of defects in other types of ultra-thin organic films on conducting surfaces.

Keywords Self-assembled monolayers · Defects · Electrochemical polymerisation · Polytyramine · Scanning tunnelling microscopy · Atomic force microscopy

Introduction

Self-assembled monolayers (SAMs) have been a very attractive research area for the past 20 years, where they have been used as model systems for fundamental studies and practical applications [1, 2, 3]. The most popular and best studied SAMs so far are SAMs of alkanethiol on gold because they offer a versatile approach for surface modification, a well-ordered monolayer, good electrochemical stability, high flexibility to attach desired functionality, and are able to fabricate complex structures using soft lithography [3, 4, 5, 6, 7, 8]. However, there are still several issues, which need to be addressed for SAMs to become more widely used. The main stumbling blocks to wider application are the presence of defects, mobility of the alkanethiol, instability at higher temperatures and oxidative or reductive desorption from surface [3, 9, 10, 11]. The defects in SAMs are particularly important where small nanometer holes, known as pinholes, are most critical [12]. These defects may alter properties of the SAMs and act as a source of erratic signals in sensing devices and molecular electronics. Therefore, considerable effort has been directed toward the fabrication of ideal and pinhole-free SAMs [3]. It has been reported that parameters such as cleanliness, thiol impurity, deposition time, and temperature have an impact on pinhole formation [3]. In our previous studies, we showed that gold topography and surface imperfections also have an influence on monolayer integrity and formation of defects [13, 14, 15, 16, 17].

Structural characterisation of SAMs defects have been reported using several techniques, including ellipsometry, electrochemistry, infrared spectroscopy, X-ray photoelectron spectroscopy (XPS), scanning electron microscopy (SEM), scanning tunnelling microscopy (STM) and atomic force microscopy (AFM) [3]. With the exception of the scanning probe microscopy (SPM) techniques, these characterisation methods provide spatial information averaged over large areas, and, as a consequence, are insensitive to individual, submicron features such as defects. SPM methods such as AFM and STM on the other hand are able to provide localised information in the form of topographic images with atomic and molecular resolution [18, 19]. Despite intensive studies over the past 10 years, the application of STM and AFM for characterisation of defects in SAMs is not always straightforward [20]. For both

D. Losic (✉) · J. G. Shapter
School of Chemistry, Physics and Earth Science,
The Flinders University, Adelaide, SA, 5001, Australia
E-mail: dusan.losic@flinders.edu.au
Tel.: +61-8-82012465
Fax: +61-8-82012405

J. J. Gooding
School of Chemistry, The University of New South Wales,
Sydney, NSW, 2052, Australia

techniques, there are still questions about the imaging mechanism, the interaction between tip and the monolayer, defect mobility, and possible artefacts. The main problem in the imaging of defects is the depth measurement of pits in monolayer, which can be ascribed to both defects in monolayer and defects on the underlying surface. STM imaging of SAMs with longer chains is difficult because it is hard to achieve stable tunnelling currents and increasing the current can also damage the monolayer. Furthermore, the origin of low tunnelling current (black holes) in STM images of SAMs is difficult to identify as the defects in the monolayer as distinct from defects on underlying surface [21, 22]. A major problem in using AFM for visualisation of defects comes from the size and shape of the AFM tip, and its inability to easily resolve small defects (less than 10 nm) and small differences in height [23, 24].

To avoid these problems in SPM characterisation of defects in SAMs, several approaches have been reported. ''Metal decoration'' is one of the methods introduced by Sun and Crooks [25, 26] based on a combination of underpotential deposition (UPD) of copper into monolayer defects and followed by STM imaging. This approach provides good results for STM but it is not applicable for AFM. ''Chemical amplifications'' was another interesting strategy reported by Whitesides et al. [27]; where an etching process (for gold and silicon) is used to convert small pinhole defects (nm scale) in the monolayer into larger pits (μm scale) of underlying metal surface. The main disadvantage of this method is the uncertainty regarding whether the etching has enlarged or increased the number of defects.

Here, we report a new approach for the visualisation of defect structures in monolayers, which combines electrochemical methods and atomic force microscopy. The approach is illustrated in Fig. 1 and can be described as ''polymer decoration''. The model of typical pinhole defects in a monolayer of alkanethiols on gold is shown at the top. To make these defects more observable for AFM imaging, the basic idea was to convert defects into three-dimensional structures. This was achieved by filling the defects by polymer using electrochemical polymerisation. The tyramine monomer is chosen for polymerisation because it gives nonconductive polytyramine (PT) film, and hence the progress of the deposition can be easily controlled [28, 29]. After polymerisation, AFM was used to directly visualise polymer structures, which corresponded to existing defects in the monolayer. This approach allows us to use the AFM for imaging of nanometer-scale pinholes and avoid problems related to the defects from the underlying surface.

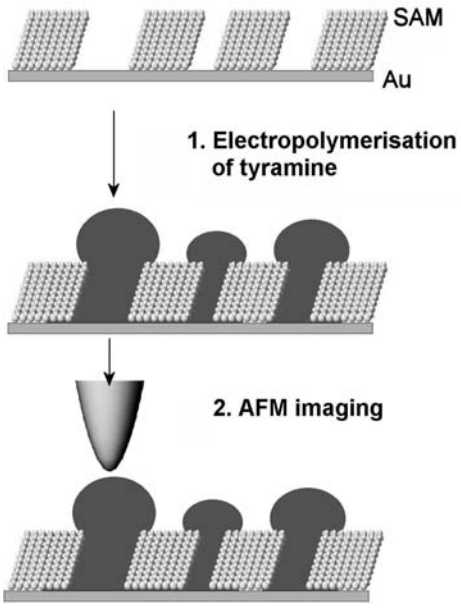

Fig. 1 Scheme of approach for mapping defects in SAMs by polymer decorating, which combines electrochemical polymerisation with atomic force microscopy

Experimental

Materials

Gold wire with 0.25-mm diameter (99.999%), 1-hexadecanethiol (HDT), and tyramine (4-hydroxyphenylethylamine) were purchased from Aldrich. Potassium ferricyanide, potassium chloride, potassium dihydrogen orthophosphate, dipotassium, and hydrogen orthophosphate, were supplied by Ajax Chem Pty. Ltd. (Sydney, Australia). The poly(dimethyl)siloxane (PDMS), brand name Silgard 184, was obtained from Dow Corning (Midland, MI, USA). Other chemicals were of the highest quality commercially available and were used without further purification. All aqueous solutions were prepared with filtered Milli Q grade water.

Preparation of SAMs on gold

Flat gold films were prepared by stripping evaporated gold from mica template using the procedure described previously [15, 30]. The flat gold samples were modified with HDT by two methods: self-assembly from solution and micro contact printing (μCP) [7, 13, 14]. In solution assembly, the gold films were exposed to 10 mM HDT in ethanol for 16 h at 25°C. For printing of HDT on gold, unpatterned PDMS stamps were prepared from Silgard 184 and printing was performed as described previously [14, 15]. After modifications, the HDT/gold samples were rinsed in ethanol followed by rinsing in water and short drying with nitrogen. Four testing spots were used from each prepared sample for electrochemical characterisation, polymerisation, and AFM imaging.

Electropolymerisation of tyramine and electrochemical characterisations

All electrochemical experiments were performed using Power Lab, Model 400 S (AD Instruments, Sydney

Australia) computer-controlled electrochemical system. Current–voltage curves were recorded on a personal computer versus an Ag/AgCl saturated KCl reference electrode and a platinum wire auxiliary electrode. Electrolyte solutions were purged with argon for at least 30 min prior to measurement and blanketed in argon throughout the experiments. All electrochemical measurements were performed at a room temperature in a purposely designed electrochemical cell, which defined the active area of the electrode using an O-ring pressed against the examined gold substrates [16].

Electrochemical polymerisation of tyramine on bare gold and HDT modified gold was performed in 0.1 M tyramine in methanol-phosphate buffer (1:3) solution. The applied potential initially used during polymerisation was between 0 and +1.3 V versus Ag/AgCl with scan rate of 0.1 and 0.5 V s^{-1}. The polymerisation was performed using between 3 and 5 cycles. After polymerisation, the samples were rinsed with methanol-phosphate buffer to remove unreacted monomer from the surface, followed by rinsing in water and drying with stream of nitrogen for 1 min. The amount of the polytyramine electrodeposited was calculated from the faradaic charge passed during tyramine oxidation. The electrochemical process is very complex, which could include the transfer of between 1 and 4 electrons during the oxidation of tyramine. It is assumed the average of two electrons for each coupling and that every oxidised tyramine species (monomer/oligomer) is precipitated on electrode surface.

The integrity of the prepared SAM-modified gold substrates before and after polymerization was assessed by two cyclic voltammetric (CV) methods: (a) probing blocking properties using a simple redox probe such as 1 mM $K_3Fe(CN)_6$ in 0.2 M KCl (applied potential was set up from −0.5 to 0.8 V versus Ag/AgCl and scan rate 0.1 V s^{-1}) and (b) determination of the pin-hole fraction areas using gold-oxide stripping experiment in 0.1 M H_2SO_4 (applied potential was from 0 to +1.5 V versus Ag/AgCl and scan rate of 0.1 V s^{-1}). In the first method, the shape of CVs and electron transfer kinetics were used for qualitative evaluation of the defects of SAMs [13, 31]. Defects in monolayers are quantitatively determined as the pinhole fraction area using the second method of gold oxide reduction peak of uncovered gold in monolayer [3, 13, 32].

SPM characterisations

SPM imaging (STM and AFM) was performed using a Digital Instruments Nanoscope IV (Veeco Corp. Santa Barbara, USA). STM images of the bare flat gold and HDT modified gold substrates were obtained in air in the constant current mode using etched tungsten tips [33]. The bias voltage was typically +0.2 V and tunnelling current set point of 3 nA for bare flat gold, and tip biases from 0.1 to 0.5 V and tunnelling currents of 60–200 pA for HDT modified gold [13]. AFM of bare flat gold and HDT/gold before and after polymerisation were performed using both tapping mode and contact mode in air. Standard silicon TESP cantilevers (Olympus, Tokyo) were used with 150–350 kHz resonant frequencies for tapping mode. Silicon nitride cantilevers with nominal spring constant 0.58–5.5 N m^{-1} were used for contact mode. Imaging was performed using "E" and "A" scanner and parameters were adjusted to obtain images with best resolution. Images with sizes of 5, 2, 1 and 0.5 μm were obtained for each substrate. Five different areas on at least three samples of each type of substrate were examined. Image processing ("bearing", grain size and profile analysis) was performed using DI off-line software (Veeco Corporation Santa Barbara, USA) and SPIP software (Image Metrology, Denmark).

Results and discussion

AFM imaging of SAMs on gold

Prior to SAM modification, the prepared flat gold films were investigated by STM and AFM in order to characterise their surface defects and imperfections. A STM image of a typical topography of bare, flat gold film is shown in Fig. 2a. The surface displays large triangular atomically flat plates separated by monoatomic steps. Its main characteristics are very low roughness (Ra < 0.1 nm) and a low density of defects (< 1%) [15, 34]. The most significant defects observed were small holes (2–20 nm in diameter, 0.2–0.7 nm deep) and long linear or curved steps. Holes are discontinuities in the gold film, and are believed to originate from incomplete coalescence during annealing. The holes may influence

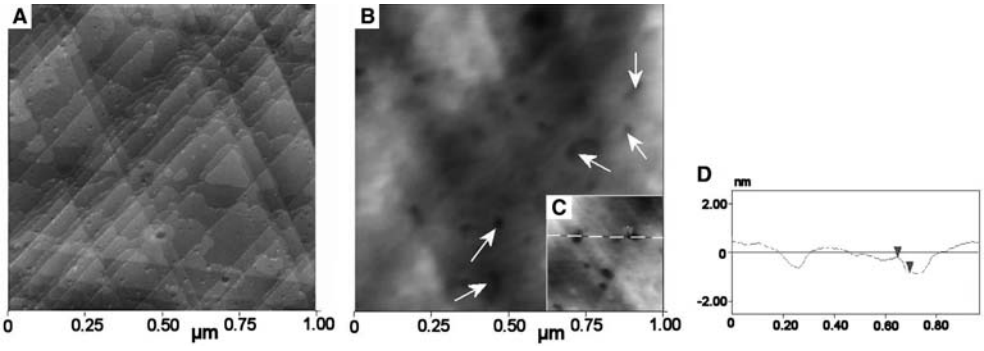

Fig. 2 **a** STM image (constant current mode in air) of flat gold prepared by stripping from mica template. **b** Topographic AFM image (contact mode in air) of HDT/gold prepared by deposition from solution. **c** High-resolution AFM image showing holes or small pits on monolayer and **d** corresponding cross section where indicated by the *dashed line* in **c**

the continuity of the SAM during assembly, resulting in monolayer defects but may also contain well-formed monolayer, which would appear as monolayer defects in SPM images [13]. It is this conundrum, which we believe the approach with polymer decoration will solve.

Flat gold films were modified with long chain alkanethiol HDT and an initial attempt to characterise defects in the monolayer using AFM is shown in Fig. 2b–d. Topographic features of the underlying gold steps can still be recognised in the image, which is a strong indication that only the monolayer is formed on the surface. Small holes and pits were observed in the monolayer and marked by arrows in Fig. 2b. A higher resolution image in Fig. 2c and corresponding cross-section graph in Fig. 2d show these holes more clearly. Their size was between 20 and 100 nm in diameter, with a depth of 0.5 to 1 nm. Similar images with holes in the monolayer were obtained from the same sample using STM (data not shown). However, STM does not allow the origin of these "holes" to be elucidating, simply indicating regions of low tunnelling current. Similarly, distinction is difficult or impossible to achieve with AFM due to the softness of the organic layer. The presented results demonstrate that SPM techniques such STM and AFM alone cannot effectively characterize defects in monolayer and that combination with other methods is needed.

Electrochemical polymerisation of tyramine on bare gold

To improve the blocking properties of defective SAMs we have demonstrated that electrochemical polymerisation to fill defects in monolayer is a useful strategy [17]. In this work, we used the same approach but with a different purpose. The polymer structures formed in monolayer defects are used to make the defects in the SAM more detectable in AFM imaging. Initial studies of electrochemical polymerisation of tyramine were performed on bare gold without a monolayer assembled. The process was carried out by cyclic voltammetry and typical CV for the polymerisation process is presented in Fig. 3. Large anodic current is observed in the first scan with a peak at +0.85 V, which decreased rapidly with the second scan and after the fifth scan, no faradaic current was observed. This reflects the passivating of the electrode by the nonconducting PT film. Very similar behaviour was found in our previous work in preparation of PT film on Pt and carbon electrodes [17, 28, 29]. The amount of the polymer formed was calculated from the faradaic charge passed during electropolymerisation and an average value of 45.2 nmol cm^{-2} was found after three cycles. This amount corresponds to about 20 layers of PT based on an average number of 8–10 monomers/nm^2.

Representative AFM images (tapping mode in air) and corresponding cross-section graphs of electrochemically formed PT film on gold are shown in Fig. 4. The film shows good adherence to the surface and uniform topography with small globular structures (Fig. 4a, b). Integrity and stability of PT film on gold surface was probed using contact mode AFM and a "scratching" method (Fig. 4c, d). The film shows resistance to removal from the surface by the AFM tip. When greater force (>50 nN m^{-1}) is used, the polymer is removed, leaving a hole in the monolayer. This experiment is used for the determination of the thickness of the polymer films. Thicknesses between 4 and 6 nm were measured as shown on the cross-section graph in Fig. 4d. The observed thickness of PT on gold exceeds the thickness of the HDT monolayer (cc 1.8 nm). This characteristic is necessary for the proposed application in mapping defects. The thickness of the electropolymerised film can be controlled by the number of potential sweeps in the cyclic voltammogram and the scan rate [28, 29]. The maximum thickness of the PT film was found to be approximately 20 nm after a high number of cycles (60–80, at 0.1 s^{-1} scan rate). This gives an idea of the maximum depth of the pinholes in the organic film (not higher than 15 nm), which could be detected by this method. Also, the low conductivity of PT is important for this approach, as it minimises the spreading of the polymer on the top of monolayer; thus allowing the polymer decoration to give a better reflection of the defect size. Similar to electrochemical polymerisation of other phenols, the oxidation of tyramine occurs through the *ortho* position and amino groups remain free [28, 29]. In general, the electropolymerisation includes two steps of nucleation and polymer growth following a very complex and not-well-understood process. Globular features of PT films observed in AFM images are a good indication of three-dimensional growth. However, comparison with electrochemical polymerisation of polypyrrole and polyamine reported in literature, PT films showed smoother topography, which is an additional reason for the choice of this polymer [35].

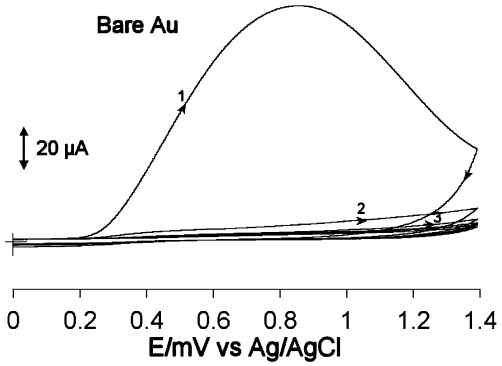

Fig. 3 Cyclic voltammogram of the electropolymerisation of tyramine on bare flat gold from aqueous 0.1 M tyramine solution (methanol phosphate buffer 1:3). Cycling potential was between 0 and 1.5 V versus Ag/AgCl and five cycles were applied using scan rate of 0.5 V s^{-1}

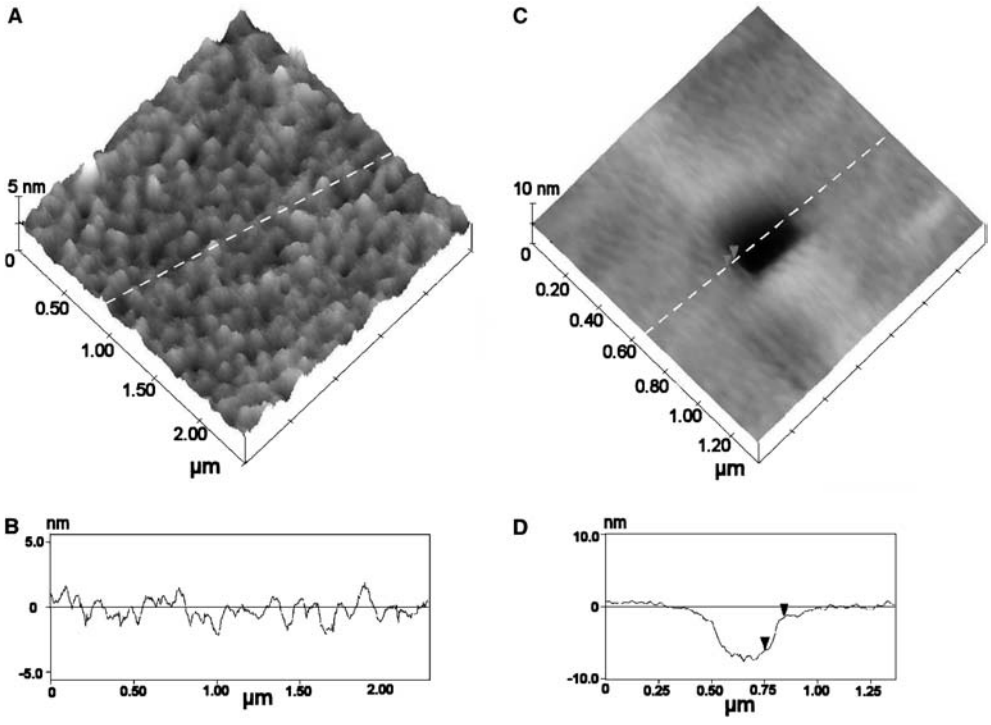

Fig. 4 **a** Typical topographic AFM image (tapping mode in air) of electropolymerised polytyramine (*PT*) film on flat gold, and **b** corresponding cross section. **c** Topographic AFM image (contact mode in air) of *PT* film obtained after scratching away a small region of polymer using high force, and **d** corresponding profile graph used for the determination of the thickness of the *PT* film

Mapping of defects in SAMs by polymer decoration

The polymerisation of tyramine was performed on selected HDT/gold samples with different numbers of defects in the monolayer. Figure 5a and b shows typical CVs of the polymerisation process of tyramine on two HDT/gold samples, with low and higher number of defects. Both CVs show much smaller anodic current in first scan and faster passivating (after second scan) than previously shown on bare gold. The small peaks in the CVs are evidence that a very small amount of tyramine is deposited on the surface, which is an indication of defects in monolayer. The first sample showed a lower anodic current than the second sample. The lower current is indicative of fewer defects in the monolayer. The oxidation process occurs at the same potential (0.8–0.9 V) as in bare gold and lowering the potential window to 0–1 V did not affect the polymerisation process. It is an advantage to apply lower potential and avoid possible desorption of weakly adsorbed SAMs during the wider potential window during cycling.

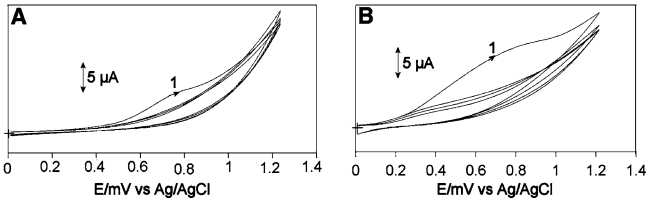

Fig. 5 Typical cyclic voltammograms of the electro polymerisation of tyramine on flat gold modified with HDT monolayer. **a** HDT/gold (assembled from solution—example of low defects SAM) and **b** HDT/gold (microcontact printing—example of high defects SAM). Cycling potential was 0–1.2 V versus Ag/AgCl, with three cycles applied at scan rate of 0.5 V s^{-1}

After polymerisation, both HDT/gold samples were characterised using AFM (tapping mode in air) and typical images are shown in Fig. 6a, d. Images show that HDT monolayer surfaces are decorated by randomly dispersed and mainly globular shaped structures. The first image (Fig. 6a) shows lower density of structures than in the second image (Fig. 6d). Control AFM experiment from HDT/gold samples before polymerisation did not show any of these structures, which suggests that observed structures are a result of the PT grown in monolayer. It is well known that long chain alkanethiol SAMs (>15 carbon groups) have excellent blocking properties against small molecules or redox probe, which cannot pass through the monolayer [3]. Therefore, it is logical to conclude that the structures observed in the images represent the polymer grown in the uncovered gold areas, which are defined by defects in the monolayer.

AFM images with polymer-decorated defects provide much useful information about SAMs defects such as their shape, size, size distribution, defect density, and their spatial distribution on surface. The shape of observed defects varied from spherical to irregular and they are isolated and randomly dispersed on surface. The profile analysis from AFM images (Fig. 6b, e) shows that the height of the polymer structures exceeds the height of monolayer (which is a prerequisite for their easy visualisation by AFM). A statistical analysis of defect size obtained from corresponding AFM images (Fig. 6a, d) are shown in Fig. 6c, f. Two different patterns of defects are observed. First, the HDT/gold

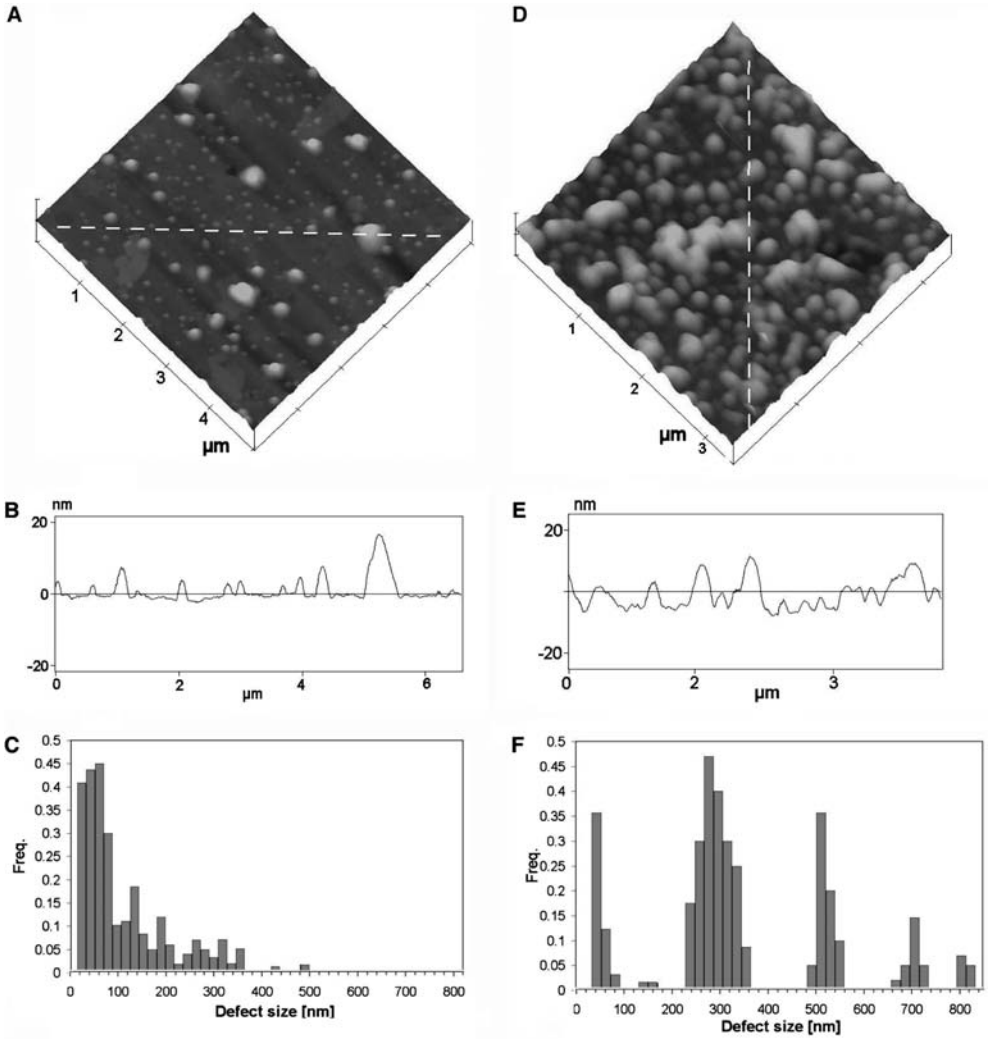

Fig. 6 Topographic AFM images (tapping mode in air) of HDT/gold monolayers with polymer (*polytyramine*) decorated defects on two typical samples, **a** HDT/gold (assembled from solution—low defects SAM), with **b** corresponding cross section and **c** corresponding defect size-distribution graph and **d** HDT/gold (microcontact printing—high defects SAM) with **e** corresponding cross section, and **f** corresponding defect size-distribution graphs

sample (Fig. 6c) shows the largest proportion of small defects with size less than 80 nm, which could be described as a less defective HDT/gold film. The second HDT/gold sample (Fig. 6f) shows larger variation of defect size from 50 to 800 nm with the highest distribution of defects with size of 200–300 nm. This sample could be described as a highly defective SAM. Mapping of smaller size defects is particularly important because they are barely detectable using the standard AFM method. The density of defects as their percentage of surface was also obtained using image processing software and defect areas of 2.7 and 32%, respectively were determined from images in Fig. 6a, d. An interesting relationship between size and height is observed. Smaller structures appear to have lower height than bigger structures. These differences are possibly related to the differences in nucleation and electron-transfer process where in small defects (less than 10 nm) polymer growth occurs with greater limitations. Polymerisation in pinholes looks very similar to the template growth of polymer in porous membranes, which is well studied and used for fabrication of nanorods and nanostructures with pores geometry (polypyrrole, polyaniline) [36]. It is expected that pinholes in monolayer act in a similar way (soft porous template) with the ability to replicate the structure of the pore through the polymerisation process. However, it is important to point out here that quantitative evaluation of topographic parameters based on AFM imaging is under question due to tip/sample convolution problems and size overestimation [23, 24]. Therefore, when quantification of data is required, particularly with structures less than 10 nm, AFM tip characterisation is essential.

Comparative characterisation of SAM defects using electrochemical methods

The presented results demonstrate that mapping of nanometer-scale defects in monolayers is achievable using the proposed method. However, the applied method still leaves several unanswered questions such as; whether polymer growth occurs on defect sites other than bare gold (collapsed monolayer, domain boundaries, steps), whether there is an overestimation of defect size due to spreading of the polymer on top of the

monolayer, whether the initiation of polymerisation by electron tunnelling through the monolayer can occur with partial desorption of the monolayer and a subsequent increase in the number of defects. In order to provide additional evidence that polymer grows exclusively on monolayer defects, such as uncovered gold, and does not cause an increase in the number of defects, a comparative electrochemical assessment of defects is performed. The same samples of HDT/gold monolayer (with different testing spots) were tested before and after polymerisation using two cyclic voltammetric methods.

In the first method, the integrity of monolayer is probed using simple redox probe such as ferricyanide. HDT/gold sample with the lower defectiveness tested before polymerisation shows a CV with sigmoidal shape (Fig. 7a). According to Amatore and Saveant theory [37], this CV shape reflects a monolayer with an array of pinholes or defects, acting as individual disc ultra microelectrodes. A characteristic of this array arrangement is that the diameter of microelectrodes is much smaller than the distance between them without overlap of their diffusion profile [3, 12]. An AFM image of the same HDT/gold sample with polymer decorated defects shows exactly the same results, small defects and large separation distance between them (Fig. 7e). Second, HDT/gold sample shows peak-shaped CV (Fig. 7b) with peak separation much higher than 60 mV (bare gold). Peak-shaped curves reminiscent of a macro electrode, are due to planar diffusion to closely spaced defect sites or large bare areas. This confirms the existence of large planar areas of bare gold in monolayer. AFM images of this sample after polymerisation show the same result: larger and densely packed defects, which are closely positioned or integrated into a very large structure (Fig. 7f). We also tested each sample after polymerisation with ferricyanide and observed the disappearance of faradaic electrochemistry in the potential region associated with ferricyanide redox chemistry. These results demonstrate that polymerised sites in monolayer correspond to defects such as uncovered gold. Electrochemical response of redox probe on other sites (e.g. collapsed SAMs) is more complex and shows more kinetic limitation in electron transfer and different CV shapes [3, 13].

An electrochemical stripping method was the second method used which is able to provide quantitative information about defects such as pinhole fraction area. The method is based on gold oxide stripping experiment in sulphuric acid [3]. In the presence of bare gold surfaces, the CV showed reduction peak obtained after stripping of formed gold oxides. Charging current from reduction peak is used for calculation of the bare gold area in the monolayer known as pinhole fraction area. [3, 12] In the first, HDT/gold sample tested before polymerisation a very small reduction peak was observed, which corresponds to small pinhole area ($1-\Theta = 0.014$) (Fig. 7c). In the second, HDT/gold sample this reduction peak was considerably higher with higher corresponding pinhole area ($1-\Theta = 0.17$) (Fig. 7d). These results are in agreement with redox probe experiments, in general, showing more extensive electrochemical process in more defective monolayer. Comparison of estimated defects using the two methods shows a slight overestimation of defect area based on polymer decoration in comparison with pinhole fraction area obtained by electrochemical method, probably due to the overestimation of polymer feature sizes due to AFM tip convolution effect [24]. However, this new method still provides a valuable approach to probe defects as extra information such as defect distributions are obtainable.

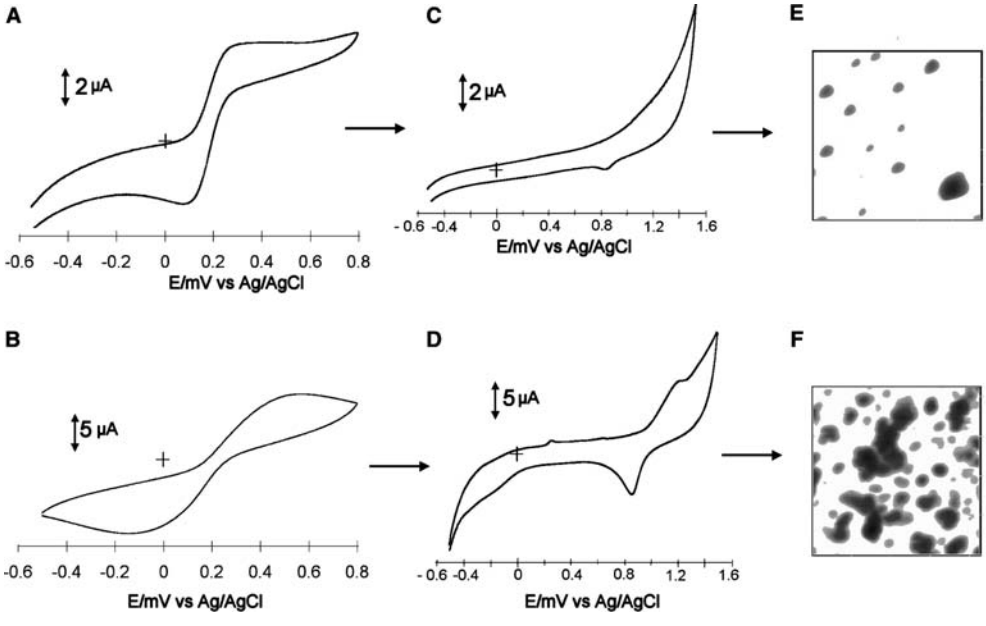

Fig. 7 Comparative electrochemical characterisation of defects in SAMs of HDT/gold. Cyclic voltammograms of HDT/gold before polymerisation in 1 mM $K_3Fe(CN)_6$ solution, **a** HDT/gold (assembled from solution) and **b** HDT/gold (microcontact printing). Cycling potential was between 0–0.8 V versus Ag/AgCl and scan rate 0.1 V s^{-1}. Cyclic voltammograms of HDT/gold before polymerisation in 0.1 M H_2SO_4, **c** HDT/gold (assembled from solution) and **d** HDT/gold (microcontact printing). Cycling potential was between 0 and 1.5 V vs. Ag/AgCl and scan rate 0.1 V s^{-1}. **e, f** Processed AFM images showing defect distribution in HDT monolayer after polymerisation with tyramine

Conclusion

A new method for mapping defects contained within SAMs of alkanethiols on gold is described. It was demonstrated that electrochemically assisted polymerisation grew a polymer on an uncovered gold surface (defects) in monolayer, and that the polymer-decorated defects can then be easily imaged by AFM. The results presented here show that by using this method, the mapping of defects in SAMs at nanoscale is achievable and the problems related to the defects from the underlying surface were avoided. The application of this method is more suitable for mapping small defects (nanometer size) rather than large defects and it is applicable only to the non-conducting polymers. Useful information such as defect shape, size, size distribution, density, and spatial distribution on surface can be obtained.

The method is demonstrated on pinhole defects with alkanethiols of self-assembled monolayers on gold, but the general approach should be suitable for characterisation of other types of ultra-thin organic films on metal surfaces such as polymers or membranes. Electropolymerised polytyramine has a free amino group, and this film is ideal for covalent attachment of a variety of biomolecules on surface [28, 29]. Particularly in combination with microcontact printing, this method offers great potential for the fabrication of complex micro and nanostructures.

Acknowledgments The authors gratefully acknowledge the Australian Research Council for aspects of this work.

References

1. Ulman A (1991) Ultrathin organic films. Academic, San Diego
2. Flink S, van Veggel FCJM, Reinhoudt DN (2000) Adv Mater 12:1328
3. Finklea HO (1996) Self-assembled monolayers of thiol electrodes. In: Electroanalytical chemistry, a series of advances, vol 19. pp109–335
4. Nuzzo RG, Allara DL (1983) J Am Chem Soc 105:4481
5. Gooding JJ, Hibbert DB (1999) TRAC 18:525
6. Gooding JJ, Mearns FJ, Yang W, Liu J (2003) Electroanalysis 15:81
7. Xia Y, Whitesides GM (1998) Angew Chem Int Ed 37:551
8. Gooding JJ, Wibowo R, Liu J, Yang W, Losic D, Orbons S, Mearns FJ, Shapter JG, Hibbert DB (2003) J Am Chem Soc 125:9006
9. Delmarche E, Michel B, Kang H, Gerber C (1994) Langmuir 9:3660
10. Finklea HO, Avery S, Lynch M, Furtsch T (1987) Langmuir 3: 409
11. Badia A, Lenox RB, Reven L (2000) Acc Chem Res 33:475
12. Finklea HO, Snider DA, Fedyk J, Sabatini E, Gafni Y, Rubinstein I (1993) Langmuir 9:3660
13. Losic D, Gooding JJ, Shapter JG (2001) Langmuir 17:3307
14. Losic D, Shapter JG, Gooding JJ (2001) Electrochem Commun 3:722
15. Losic D, Shapter JG, Gooding JJ (2001) Aust J Chem 54:643
16. Losic D, Gooding JJ, Shapter JG, Hibbert DB, Short K (2001) Electroanalysis 13:1385
17. Losic D, Shapter JG, Gooding JJ (2002) Electrochem Commun 4:953
18. Butt H-G, Seifert, Bamberg E (1993) J Phys Chem 97:7316
19. Poirier GE (1997) Chem Rev 97:1117
20. McCarley RL, Dunaway DJ, Willicut RJ (1993) Langmuir 9:2775
21. Han T, Beebe TP Jr (1994) Langmuir 10:2706
22. Sondag-Huethorst JAM, Schönenberger C, Fokkink LGJ (1994) J Phys Chem 98:6826
23. Schwarz UD, Haefke H, Reimann P, Gőntherodt H-J (1994) J Microscopy 173:183
24. Losic D, Short K, Gooding JJ, Shapter JG (2004) J Serb Chem Soc 69:93
25. Sun L, Crooks RM (1991) J Electrochem Soc 138:L23
26. Sun L, Crooks RM (1993) Langmuir 9:1951
27. Zhao Z-M, Wilbur JL, Whitesides GM (1996) Langmuir 12:3257
28. Situmorang M, Gooding JJ, Hibbert DB, Barnett D (1998) Biosens Biolectron 13:953
29. Situmorang M, Gooding JJ, Hibbert DB, Barnett D (2001) Electroanalysis 13:1469
30. Mazurkiewiecz J, Mearns FJ, Losic D, Rogers C, Gooding JJ, Shapter JG (2002) Vac Sci Techn B 20:2265
31. Porter MD, Bright TB, Allara D, Chidsey CED (1987) J Am Chem Soc 109:3559
32. Sabatini E, Rubinstein I, Maoz R, Sagiv J (1987) J Electroanal Chem 219:365
33. Rogers BL, Shapter JG, Skinner WM, Gascoigne K (2000) Rev Sci Instrum 71:1702
34. Losic D, Shapter JG, Gooding JJ (2002) Langmuir 18:5422
35. Hwang B-J, Santhanam R, Lin Y-L (2003) Electroanalysis 15:115
36. Delvaux M, Duchet J, Stavaux P-Y, Legras R, Demoustier-Champagne S (2000) Synthetic Metals 113:275
37. Amatore C, Savéant JM, Tessier D (1983) J Electroanal Chem 147:39